

Regular article

Bifurcation of reaction pathways: the set of valley ridge inflection points of a simple three-dimensional potential energy surface

Wolfgang Quapp¹, Michael Hirsch¹, Dietmar Heidrich²

¹Mathematisches Institut, Universität Leipzig, Augustus-Platz, D-04109 Leipzig, Germany

²Institut für Physikalische und Theoretische Chemie, Universität Leipzig, Augustus-Platz, D-04109 Leipzig, Germany

Received: 8 July 1998 / Accepted: 24 August 1998 / Published online: 23 November 1998

Abstract. This paper serves for the better understanding of the branching phenomenon of reaction paths of potential energy hypersurfaces in more than two dimensions. We apply the recently proposed reduced gradient following (RGF) method for the analysis of potential energy hypersurfaces having valley-ridge inflection (VRI) points. VRI points indicate the region of possible reaction path bifurcation. The relation between RGF and the so-called global Newton search for stationary points (Branin method) is shown. Using a 3D polynomial test surface, a whole 1D manifold of VRI points is obtained. Its relation to RGF curves, steepest descent and gradient extremals is discussed as well as the relation of the VRI manifold to bifurcation points of these curves.

Key words: Three-dimensional potential energy surface – Reaction path bifurcation – Valley-ridge inflection – Reduced gradient following – Gradient extremal

1 Introduction

The concept of the minimum energy path (MEP) or reaction path (RP) of a potential energy surface (PES) is the usual approach to the theoretical kinetics of larger chemical systems [1]. Reaction theories are based either implicitly (transition state theory [1]) or explicitly (variational transition state theory [2]) on the knowledge of the RP. The RP is defined as that line in the configuration space which connects the reactant and the product minimum by passing the saddle point (SP) of an adiabatic PES. The SP (the transition structure) and the minima form stationary points of the PES.

Frequently, RP branching occurs. The corresponding points are the so-called bifurcation or branching points (BPs). The mathematical description of RP branching is of high theoretical interest, and it is one of those ques-

tions which now requires closer consideration in quantum chemistry. Many procedures – although mostly developed in mathematics – are not yet adapted for use in quantum chemistry, though there are a number of recent studies dealing with aspects of the definition of RPs and their bifurcation [3–16].

The choice of a path for a chemical reaction is a complex issue. It is important to state that a BP is a component of the particular RP definition and, therefore, a bifurcation of the RP generally will be found by the BP of those particular curves selected to calculate the MEP. Bifurcations of the path may be caused by symmetry breaking [17]. Then, two or more equivalent pathways may lead over equivalent transition structures to two or more equivalent (or chiral) products. It is helpful to consider that RP branching (symmetric or unsymmetric) is more often than not connected with the emergence of a special class of points of the PES, the valley-ridge inflection (VRI) points [3, 4]. The traditional definition is that a VRI point is that point in the configuration space where, orthogonally to the gradient, at least one main curvature of the PES becomes zero. Thus, VRI points can be defined independently of a RP definition. They are, in general, not identical with BPs of different RP definitions, although both are often adjacent points. Usually, VRI points represent non-stationary points of the PES. “Adjacent” means that no other point of mathematical interest lies in between.

Before we present an algorithm to locate VRI points, we analyse the potential of the usual RP following to locate bifurcations. The mathematically most simple RP definition is the steepest descent from an SP, resulting in the well-known intrinsic reaction coordinate (IRC) of Fukui [18–20]. This pathway is defined by an autonomous system of differential equations for a tangent vector along the curve searched for. Its solution is unique. Therefore, if starting at any initial point outside an SP, no bifurcation can occur before reaching the next stationary point. Hence, no branching of PES valleys will be truly described by following the IRC; see the discussion in [11, 12]. However, following an IRC we may test the curvatures orthogonal to the path, thus

Correspondence to: W. Quapp
e-mail: quapp@serverl.rz.uni-leipzig.de

orthogonal to the gradient of the potential – and so detect a VRI region [21].

Gradient extremals (GEs) form a second approach for RP following [7–9, 22–27]. They are more complicated than the IRC, but better fitted to solve the valley branching problem. However, other problems arise owing to the occurrence of pairs of turning points instead of the BP. Such turning points may interrupt the pathway between the minimum and the SP. The GE curves often show some kind of avoided crossing [8, 9, 23]. The BP indicated by a valley GE is that point where the valley usually branches into three valleys [7] – and, usually, it does not branch into two valleys with a ridge in between, as is assumed at a VRI point. Because there are cases of missing the BP owing to turning points, GE bifurcation is a sufficient but not a necessary condition for the occurrence of branching along a RP. Nevertheless, the whole turning point region of two related GE curves has to be considered as a branching region of a valley (or of a ridge). The BP condition for GEs contains third derivatives of the PES, and it does not require a singular Hessian [24]. This indicates that in the general case the BP of GEs are not the VRI points of the surface, and GE bifurcation can occur without a nearby VRI point.

A third approach to the problem of finding the reaction path branching is quite different. It deals with the direct location of the VRI points [10, 16, 21] which, up to now, are always understood to be single points in the configuration space. Here, the geometrical imagination is clear: the valley-ridge inflection is that place where an eigenvalue of the Hessian orthogonal to the gradient direction changes from “+” to “–” through zero, or vice versa. A valley inflects into a ridge. The zero eigenvalue of the Hessian, orthogonal to the valley direction, is relatively easy to detect, at least in symmetric PES regions. There are some proposals dealing with this task [21]. An explanation is already given for the emergence of VRI in formaldehyde-like molecules by the second-order Jahn-Teller effect [16].

In order to determine the VRI – and in this way also the BP of RP – we recently proposed the reduced gradient following (RGF) procedure on the PES [28]. RGF consequently continues the old method of a distinguished coordinate (or coordinate driving) and replaces the energy optimization of the residual coordinates by the solution of a reduced gradient system with a Newton-Raphson step. It is much simpler to realize in comparison with the GE following [24, 27]. RGF needs gradient and (updates of) the Hessian of the PES. It gives a network of curves which contain in most cases all stationary points of the PES; the method is used to effectively find stationary points [28]. Interestingly enough, the BPs of these curves are fortunately the VRI points of the PES. So, by tracing suitable RGF curves, VRI points of the PES may be located! We incorporated the method for the n -dimensional case into our version of the GAMESS-UK program [29].

In this paper we present a model PES with three coordinates (x, y, z), thus having four dimensions. We only use linear, quadratic, quartic and mixed terms for the three degrees of freedom. We refer to the fact that the PES of triatomic molecules is three-dimensional (3D) in

internal coordinates. However, we use a test surface rather than a real molecule’s PES to demonstrate the fundamental properties of bifurcation points by the analytical formulas of the surface. In this manner we avoid the use of “unsafe” numerical results of quantum chemical calculations. In addition, a symmetric surface is chosen leading to symmetric BPs. The objective of the paper is (1) to show the VRI/BP determination by RGF for the 2D case, (2) to demonstrate the changes when going from two coordinates to a third dimension, and (3) to show the possibilities of a combined use of RGF and GE in order to characterize branching regions.

The paper is organized as follows. First, we illustrate the fundamentals and algorithms of the RGF method [28], and the so-called global Newton method [30] which is mathematically strongly related to RGF. RGF curves, as well as global Newton solutions, are extensively explained using the example of this paper. The VRI points found are then discussed in relation to BPs found by GEs. A set of illustrations is given to introduce the reader to the representations of the 3D coordinate space plus one dimension of the surface.

2 The reduced gradient idea

The chemically most important features of the PES are the reactant and the product minimum and the SP in between. These stationary points of the PES are characterized by the condition

$$\nabla E(\mathbf{x}) = 0, \quad (1)$$

when $E(\mathbf{x})$ is the function of the PES, and $\nabla E(\mathbf{x})$ is its gradient vector in the configuration space, \mathbf{R}^n , defined by the coordinates \mathbf{x} of the molecule where $n = 3N$ (N = number of atoms) if Cartesian coordinates are used, or $n = 3N - 6$ for internal coordinates. Thus, we use n to indicate the dimensionality of the problem, in this paper 3; \mathbf{x} and $\nabla E(\mathbf{x}) = \mathbf{g}$ are vectors of the dimension n . Recently, the old distinguished coordinate method [31, 32] was transformed into a new mathematical form [28]. Equation (1) is valid at extrema of the PES, but single components of the gradient can also vanish in the neighbourhood of an extremum, as well as in other regions of the PES. Using this property, a curve of points \mathbf{x} is followed which fulfill the $n - 1$ equations

$$\frac{\partial E(\mathbf{x})}{\partial x^i} = 0, \quad i = 1, \dots, k, \dots, n \quad (2)$$

omitting the k th equation [28, 32]. This gives the $(n - 1)$ -dimensional zero vector of the reduced gradient; the method is subsequently called reduced gradient following (RGF). Equation (2) means that the gradient points in the direction of the pure x^k coordinate. The concept may be generalized by the challenge that any selected gradient direction is fixed

$$\nabla E(\mathbf{x}) / \|\nabla E(\mathbf{x})\| = \mathbf{r}, \quad (3)$$

where \mathbf{r} is the selected unit vector of the search direction, as shown below.

The idea of the method may be explained using the surface [4, 14, 15] shown in Fig. 1

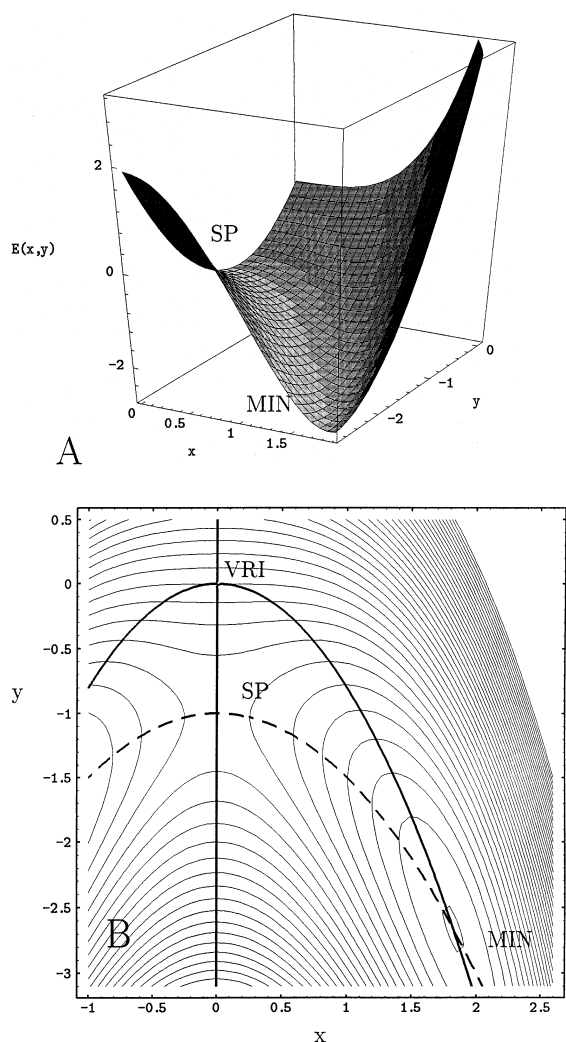


Fig. 1A, B. 2D model potential surface $E(x, y) = 2y + y^2 + (y + 0.4x^2)x^2$ with the RGF curves $E_x = 0$ (bold faced) or $E_y = 0$ (dashed). The curves connect minima, MIN, with the saddle point, SP. Their intersection locates the three stationary points as well as the VRI point which is a BP of the $E_x = 0$ curves

$$E(x, y) = 2y + y^2 + (y + 0.4x^2)x^2, \quad (4)$$

where now x and y are used as the coordinates. It has three stationary points: two minima, MIN ($\pm\sqrt{10/3}, -8/3$), and the SP (0, -1). A MEP (may be an isomerization) connects two equivalent minima crossing the SP. A further MEP (possibly being a dissociative pathway) can be thought of starting at the SP and running along the positive y axis; cf. also [15] for a “chemical interpretation” of such a PES and further references. The RGF equations become

$$\begin{aligned} E_x(x, y) &= 2xy + 1.6x^3 = 0, & \text{Eq. (2) for } k = 2 & \\ E_y(x, y) &= 2 + 2y + x^2 = 0, & \text{Eq. (2) for } k = 1, & \end{aligned} \quad (5)$$

with the three solution curves $x = 0$ and $y = -0.8x^2$ for $E_x = 0$, or $y = -0.5x^2 - 1$ for $E_y = 0$. They are illustrated in the lower panel B of Fig. 1 using the program Mathematica [33]. The reduced gradient curve $E_x(x, y) = 0$ intersects the equipotential lines in those

points where their tangents are parallel to the x axis. Thus, the gradient at these points in the y direction is: $\nabla E = (0, E_y)$. RGF is a simple but effective procedure in order to determine all types of stationary points [28]. Unlike the usual steepest descent path from a saddle, the reduced gradient search for a fixed k locally has an explicit analytical definition. By the choice of k between 1 and n in Eq. (2) we obtain n different RGF curves where, in the general good-natured case, each of them passes each stationary point. We must recall that these curves usually are not minimum energy paths. They are defined by the shape of the PES in the given coordinate system, and by the character of the gradient vector between the extrema. Nevertheless, these curves may follow a reaction valley in favourable cases, at least qualitatively. For example, the RGF curve $E_y = 0$ in Fig. 1B (dashed) approximates the RP between SP and MIN. On the other hand, the point (0, 0) on the RGF curve $E_x = 0$ is a VRI point of the surface heading in the dissociative direction of the y axis. Here, a MEP coming from positive y values bifurcates to the left or to the right minimum. The part of the y axis between the points (0, 0) and (0, -1) is a crest of a bluff (with the notation of [24]). The VRI point satisfies the necessary condition of orthogonality of the two vectors included in its definition (cf. [21])

$$\mathbf{g}^T \mathbf{e}_0 = 0 \quad (6)$$

for an eigenvector \mathbf{e}_0 of \mathbf{H} with zero eigenvalue and for the gradient \mathbf{g} (the upper index “ T ” means the matrix transposition). The VRI point (0, 0) is simultaneously the bifurcation point of the two branches of the RGF curve existing for $E_x = 0$. The bifurcation of the RGF curve, $E_x = 0$, shows the typical pattern of a so-called pitchfork bifurcation.

The RGF approach shows an important analogy to the mathematical theory of Branin [34], the global Newton method [30]. It utilizes the adjoint matrix \mathbf{A} of the Hessian \mathbf{H} . This is defined as $((-1)^{i+j} m_{ij})^T$ where m_{ij} is the minor of \mathbf{H} obtained by deletion of the i th row and the j th column from \mathbf{H} , and taking the determinant. The adjoint matrix \mathbf{A} is used to define an autonomous system of differential equations for the curve $\mathbf{x}(t)$, where t is a curve length parameter:

$$\frac{d\mathbf{x}}{dt} = \mp \mathbf{A}(\mathbf{x}) \mathbf{g}(\mathbf{x}). \quad (7)$$

Thus, the tangent of the curve of interest does not point in the direction of the gradient, as is the case using the IRC. The tangent is the gradient \mathbf{g} of the PES transformed by the adjoint matrix \mathbf{A} . The “+” option is used for searching stationary points with odd index (SPs with an odd number of negative eigenvalues of the Hessian), where the “-” option searches for stationary points with even index (minima, or SPs with an even number of negative eigenvalues of the Hessian). Stationary points of the PES are limit points of the solution, because there $\mathbf{g} = \mathbf{0}$. However, there are further possible limit points, or fix-points, also in regions with $\mathbf{g} \neq \mathbf{0}$. These are points where

$$\mathbf{A}(\mathbf{x}) \mathbf{g}(\mathbf{x}) = \mathbf{0}. \quad (8)$$

Because of the possible zero vector (8) in (7), the bifurcation of solution curves can take place somewhere at the slope of the surface, where $\mathbf{g} \neq 0$. In Appendix A, the proof is given that the BP of a Branin curve is a VRI point also fulfilling definition (6). [In Appendix B we additionally report that the definitions (8) and (6) are also fulfilled by a manifold of cusp points of equipotential lines.] Points which satisfy Eq. (8) are named extraneous singularities [30] of Eq. (7) because they are possible numerical perturbations of the search for stationary points. Because of the property of the adjoint

$$\mathbf{H}\mathbf{A} = \text{Det}(\mathbf{H})\mathbf{I}, \quad (9)$$

where \mathbf{I} is the n -dimensional unit matrix, we obtain for the non-singular case, if \mathbf{H}^{-1} exists, the system

$$\frac{d\mathbf{x}}{dt} = \mp \mathbf{H}^{-1}(\mathbf{x}) \mathbf{g}(\mathbf{x}) \text{Det}(\mathbf{H}) \quad (10)$$

instead of Eq. (7). This represents a Newton step with a damping factor $\text{Det}(\mathbf{H})$. Curves satisfying this expression are called Newton flows. Solution curves of Eq. (7) have a special character. Considering the behaviour of the gradient $\mathbf{g}(\mathbf{x}(t))$ along a solution, $\mathbf{x}(t)$, we obtain with (7) and (9)

$$\frac{d\mathbf{g}}{dt} = \mathbf{H} \frac{d\mathbf{x}}{dt} = \mp \mathbf{H}\mathbf{A}\mathbf{g} = \mp \text{Det}(\mathbf{H})\mathbf{g}. \quad (11)$$

Thus, the gradient \mathbf{g} changes proportionally to \mathbf{g} itself. This means that the direction of \mathbf{g} does not change. It is invariant along the solution. On the other hand, also $(n-1)$ orthogonal directions \mathbf{e}_i to \mathbf{g} can be chosen constant along a solution. Directional derivatives along these directions of the surface vanish because the surface is always orthogonal to its gradient:

$$\frac{\partial E}{\partial \mathbf{e}_i} = 0, \quad i = 1, \dots, n-1. \quad (12)$$

This system of equations leads to the RGF, Eq. (2), if we use \mathbf{g} and \mathbf{e}_i as basis vectors in Eq. (2) (cf. also Sect. 3 for a more general search direction of a RGF equation).

From another point of view, the RGF equation gives an alternative definition of the Newton flows in comparison with Eq. (7). The two strategies, RGF and global Newton method, are slightly different with respect to their initial conditions. The RGF method, Eq. (2) or Eq. (16) below, is started at stationary points with a well-defined initial direction of the gradient search, whereas the Branin differential equation, Eq. (7), may start anywhere on the PES but outside a stationary point using the gradient direction of that point. So, the Branin algorithm may easily stop anywhere, and continue using the gradient of that point.

3 The algorithm for RGF

3.1 Predictor step

We assume a curve of points, $\mathbf{x}(t)$, fulfilling the $n-1$ equations

$$\frac{\partial E(\mathbf{x}(t))}{\partial x^i} = 0, \quad i, \dots, k, \dots, n, \quad (13)$$

however

$$\frac{\partial E(\mathbf{x}(t))}{\partial x^k} \neq 0 \text{ outside stationary points.}$$

The parameter t varies in a certain interval. If Eq. (13) can be solved analytically, it gives the RGF curves. If we need a numerical solution, the starting point may be any stationary point, for example, a minimum. To predict the next point, we calculate the tangent to the curve [35]. It is given by

$$\frac{d}{dt} \frac{\partial E(\mathbf{x}(t))}{\partial x^i} = 0 = \sum_{l=1}^n \frac{\partial^2 E(\mathbf{x})}{\partial x^i \partial x^l} \frac{dx^l(t)}{dt} \quad i = 1, \dots, k, \dots, n$$

or

$$\widehat{\mathbf{H}}\mathbf{x}' = \mathbf{0}. \quad (14)$$

It is a homogeneous system of $n-1$ linear equations for the direction cosine of the n components dx^l/dt of the tangent, \mathbf{x}' . The coefficients are entries of the Hessian matrix $\widehat{\mathbf{H}} = \partial^2 E(\mathbf{x})/\partial x^i \partial x^l$ where the $i = k$ th row is omitted. The algorithm [28, 35] uses QR decomposition of the matrix of system (14) to obtain the solution. (\mathbf{Q} is an orthogonal matrix, \mathbf{R} is an upper triangular matrix.) The calculation of the Hessian may be replaced by the DFP update procedure [9, 28]. If internal coordinates are used, then the corresponding formulas of the metric tensor have to be included [9, 19, 36].

There is an alternative and more general way to define a RGF curve. To follow a gradient in any fixed direction \mathbf{r} we construct the projector \mathbf{P}_r with the property

$$\mathbf{P}_r^T \mathbf{r} = \mathbf{0}, \quad (15)$$

where the columns of \mathbf{P}_r and $\mathbf{r}/\|\mathbf{r}\|$ form an orthonormal base. The equation

$$\mathbf{P}_r^T \nabla E(\mathbf{x}(t)) = \mathbf{0} \quad (16)$$

describes a curve with gradients of the constant direction \mathbf{r} in each of its points. The tangents to these curves are given by

$$\frac{d}{dt} \mathbf{P}_r^T \nabla E(\mathbf{x}(t)) = \mathbf{P}_r^T \mathbf{H}(\mathbf{x}(t)) \mathbf{x}'(t) = \mathbf{0} \quad (17)$$

This again is a homogeneous system of $n-1$ linear equations for n components of \mathbf{x}' .

The predictor step is

$$\mathbf{x}_{m+1} = \mathbf{x}_m + \frac{\text{StL}}{\|\mathbf{x}'_m\|} \mathbf{x}'_m \quad (18)$$

where \mathbf{x}_{m+1} is the next point, \mathbf{x}'_m is the solution of Eq. (14) or Eq. (17), correspondingly, and the steplength, StL, is used as a parameter. For example, the distinguished coordinate takes StL = 0.1 units (Å, rad) in the case of the four-atomic H_2CO , and 0.2–0.6 units for tetrazole with seven atoms [28].

It is quite normal for any RGF that turning points may occur [32]. Using the tangent search, Eq. (14) or

(17), the algorithm overcomes turning points without problems. If, at any point arrived at by RGF, Eq. (13) or (16) is fulfilled to a given tolerance, the next predictor step is executed, otherwise the algorithm skips to the corrector.

3.2 Corrector step

A Newton-Raphson-like method is used to solve the reduced system of Eq. (13) or (16). The steplength of this method is intrinsically given, and it is used until convergence. However, in addition we impose an upper limit of the steplength, because if a BP is touched, the pure Newton corrector produces too large steps. The tolerance is taken to be $0.1 \times (\text{predictor StL})$.

3.3 Stopping criterion

At every point along RGF, we determine the hypothetical steplength of the Newton step towards the “next” stationary point. If this value falls below a given tolerance, say $(0.5 + \epsilon) \times (\text{predictor StL})$, the algorithm still carries out this step and then stops.

4 The algorithm for the Branin method

4.1 Step search

We choose a StL parameter and discretize the system (7) to

$$\mathbf{x}_{m+1} = \mathbf{x}_m \mp \text{StL} \mathbf{A}_m \mathbf{g}_m \quad (19)$$

where \mathbf{m} is the step number, as before. For example, in the case of the four-atomic H_2CO , we use $\text{StL} = 100$ units of the corresponding coordinate (\AA , rad) for a satisfactory exploration along the Newton flow. Because of the self-correcting definition, we do not need the corrector. If a special symmetry shall be conserved along a Newton flow, we enforce a symmetrization of the next step.

4.2 Stopping criterion

If the hypothetical steplength of the Newton step towards the “next” stationary point falls below a given tolerance, the algorithm stops. Note: the gradient in algorithm (19) becomes small near stationary points. This would cause inefficient small steps near stationary points. The effect is avoided by an automatic increase of the steplength.

4.3 Search of VRI points

The Branin method can also be used to search for VRI points. One important condition is the strict symmetry constraint. When starting anywhere in the coordinate space, a Branin curve may almost reach the VRI point;

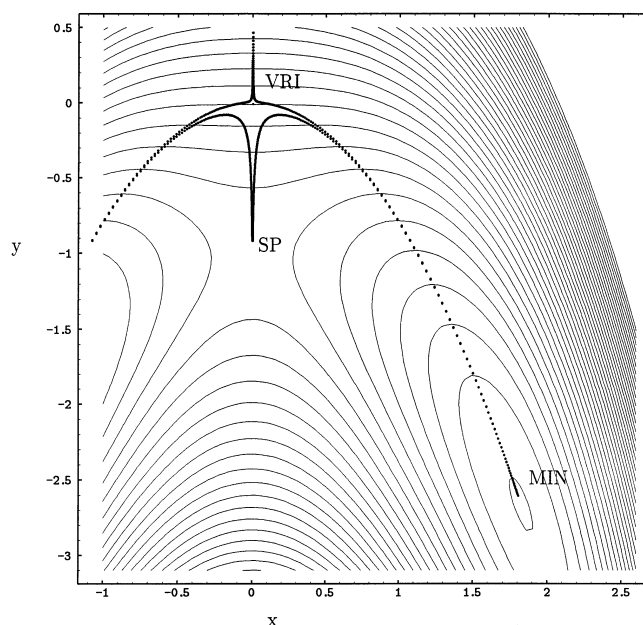


Fig. 2. Numeric solutions of the Branin differential equation. The curves begin somewhere beside the symmetry axis $x = 0$. They bypass the VRI point, $(0,0)$, like gradient curves pass a saddle point

however, usually it turns off by passing this point. This is shown in Fig. 2 for four Branin solutions of the surface Eq. (4); see also below. The example demonstrates the general behaviour of Branin solutions: they connect stationary points of different index, or they end in a VRI point. The point where a Branin solution turns off is a turning point (TP). The occurrence of a TP may suggest the nearby existence of a VRI point.

5 Gradient extremals

A point showing the gentlest ascent of a valley is defined by the condition that the norm of the gradient forms a minimum taken along an equipotential surface, $E(\mathbf{x}) = \text{const.}$, i.e. in all directions perpendicular to the gradient [14, 22, 23]. It results in the basic eigenvector relation

$$\mathbf{H}(\mathbf{x}) \cdot \mathbf{g}(\mathbf{x}) = \lambda(\mathbf{x}) \mathbf{g}(\mathbf{x}) \quad (20)$$

The proportional factor $\lambda(\mathbf{x})$ is an eigenvalue of the Hessian, and the gradient is its eigenvector. Note the difference of Eq. (20) in comparison to the VRI orthogonality requirement of Eq. (6). In the GE definition (20) the gradient has to be an eigenvector, while in Eq. (6) it only has to be orthogonal to a special other eigenvector. Thus, the gradient is not required to be an eigenvector at a VRI point! Curves defined by (20) consisting of such points on consecutive equipotential hypersurfaces are termed gradient extremals [23]. However, following a curvilinear GE implies that one actually does not move in the direction of the gentlest ascent [14, 23]. The measure for the ascent of the n -dimensional PES functional $E(\mathbf{x})$ is the norm of the gradient vector $\mathbf{g} = (g_1, \dots, g_n)$, or expedient for calculation, the functional

$$\sigma(\mathbf{x}) = \frac{1}{2} \|\mathbf{g}(\mathbf{x})\|^2 \quad (21)$$

The GE Eq. (20) selects all points of the configuration space having an extreme value of $\sigma(\mathbf{x})$ with respect to variations on equipotential surfaces. So, if $\sigma(\mathbf{x})$ has a minimum the PES may show a valley-floor GE; however, it may also be a crest of a ridge. The extremes of $\sigma(\mathbf{x})$ can also be maxima or degenerate stationary points [9, 14, 24]. Hence the GE following suffers from the ambiguity of the GE character.

Formula (20) forms a system of n equations of rank $n - 1$ with n unknown variables x^1, \dots, x^n . For curve tracing, we need therefore $n - 1$ independent equations. From the extremum definition of GE, it follows that the $n - 1$ directional derivatives have to vanish:

$$\text{GE}_i(\mathbf{x}) := \frac{\partial \sigma}{\partial \mathbf{e}_i} = 0, \quad i = 1, \dots, n - 1 \quad (22)$$

In Eq. (22), the same i directional derivatives orthogonal to the gradient of $E(\mathbf{x})$ are used, as well as in Eq. (12). Despite the computational problems, GEs are often used to describe valley ground pathways and their branching. However, BPs of a GE are in general not identical with the VRI points of the PES; see [14].

6 Test surface in R^3

6.1 Presentation of a 3D test PES

Example (4) is now extended to three dimensions by adding a quadratic and a mixed term for the z -direction:

$$E(x, y, z) = 2y + y^2 + (y + 0.4x^2 + z^2)x^2 + 0.01z^2 \quad (23)$$

It has, for $z = 0$, the same stationary points as surface (4), and further stationary points do not emerge. The surface is a simplified version of a higher-dimensional molecular PES, related to malonaldehyde-like systems [4, 37, 38]. In the case of proton transfer in malonaldehyde, x is the displacement of the H atom, $-y$ is the symmetric O–O stretch, and z may be the out-of-plane wagging motion of the molecule (the z^2 term has for the molecular PES a larger factor). We are not able to draw the full 4D problem. Hence, usually, 2D sections of the full PES are interpreted. For $z = 0$, Eq. (23) reduces to Eq. (4) depicted in Fig. 1. In Fig. 3 we display a series of sections for the planes $z = 0.5$, $z = 1$ and $z = 1.5$. There is a qualitative change of the surface features. The two symmetric minima in panel A flow together to one 2D “banana” minimum at $x = 0$, $y = -1$, $z = 1$ in panel B. The 2D minimum is “degenerate” at this point, because the surface is in the x direction pure quartic. In panel C, the region around the minimum at $z = 1.5$ has the convex shape of a bowl. At all points $z \neq 0$ there is a positive slope of the gradient (24) in the z component. Thus, all stationary points in the 2D sections are somewhere at a slope of the 3D surface.

The 2D RGF curve, $E_y = 0$ (dashed in Fig. 3), is similar for all cuts with $z = \text{constant}$ [owing to the simple form of the surface (23)]. The example is chosen for the nice behaviour of the bifurcating 2D RGF solution,

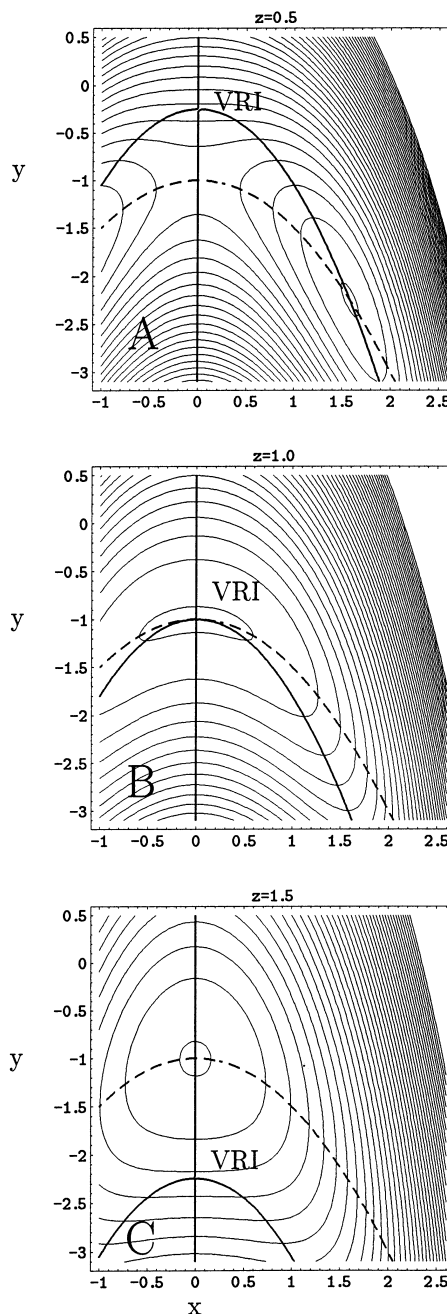
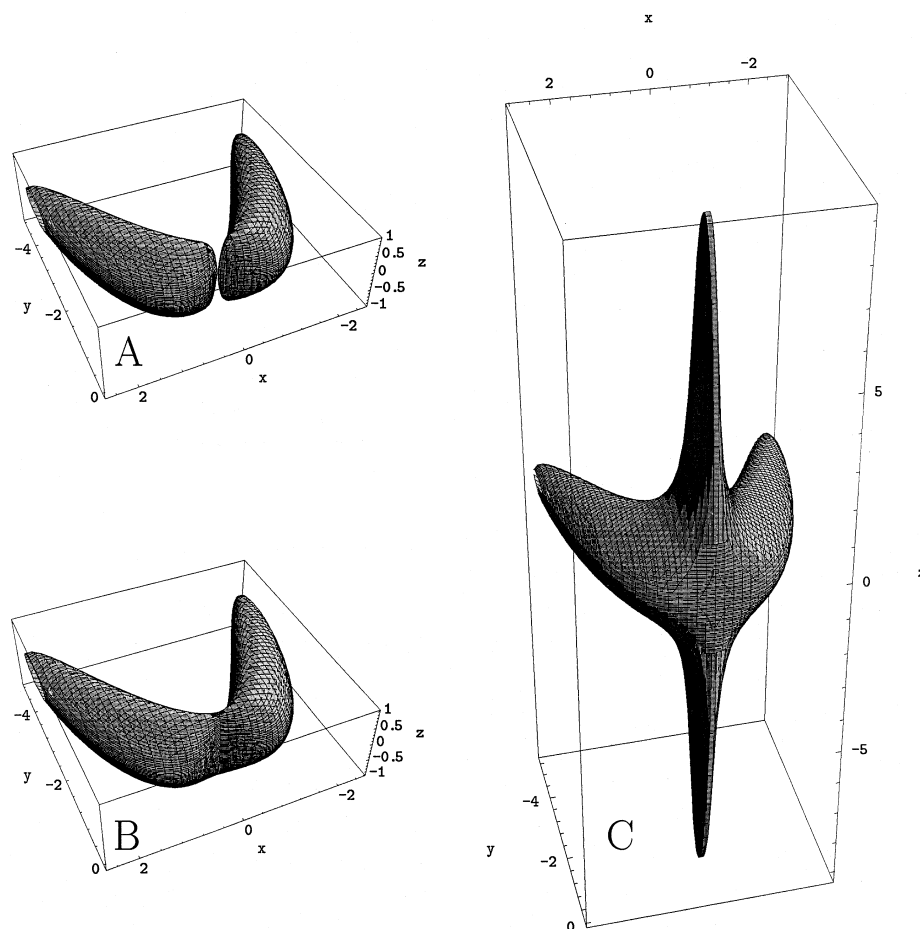


Fig. 3. 2D sections of (x, y) planes of the 3D polynomial surface $E(x, y, z) = 2y + y^2 + (y + 0.4x^2 + z^2)x^2 + 0.01z^2$ at **A:** $z = 0.5$; **B:** $z = 1.0$; and **C:** $z = 1.5$. (The case $z = 0$ is already given in Fig. 1.) Note: $z = 1$ in panel **B** marks a qualitative change of the surface in full R^3

$E_x = 0$. Its BP runs down along the y axis with increasing z . For $z = 0$ it is at zero y , for $0 < z < 1$ it is at $-1 < y < 0$, for $z = 1$ it collapses exactly with the degenerate minimum and for $z > 1$ it turns to the other side of the minimum with $y < -1$.

In Fig. 4, the PES is additionally characterized by some equipotential surfaces of function (23) in 3D which corresponds to equipotential lines in 2D sections. Chosen are the values $E(x, y, z) = -1$ in panel A, $E = -0.99$

Fig. 4A–C. Equipotential surfaces of the 3D surface of Fig. 3 at **A:** $E = -1$ through the SP; **B:** $E = -0.99$; and **C:** $E = 0.0$ through the BP above the SP



in B and $E = 0$ in C. A set of “body-shapes” for increasing energies like those in Fig. 4 is well suited to give insights into the forms of 3D coordinate influenced modes of the molecule. The surface of case A touches the SP of the full 3D surface (23) at point $(0, -1, 0)$. Panel B contains the two global BPs $(0, -1, \pm 1)$ (see below); the surface of case C passes through point $(0, 0, 0)$, being also a global BP with VRI character. The three equipotential surfaces are nested like onion skins: A in B, and B in C. The two global MIN of the 3D PES are lying symmetrically inside the lobes of the 2D equipotential surface A.

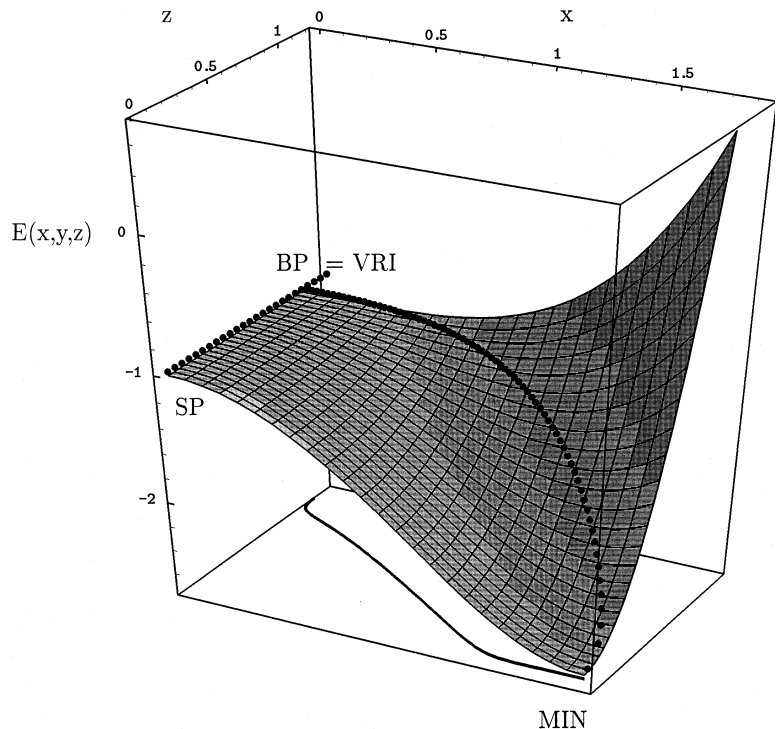
If we assume a molecule vibrating with a given energy, then the geometry change of the molecule under the vibration would remain within the equipotential surface of the given energy. If we further assume a molecule vibrating for example slowly with z , we get for every fixed z , thus using a z section, a “breathing” PES in the other two dimensions, maybe quickly vibrating modes in a corresponding x, y plane; cf. Fig. 3. However, the breathing is quite complicated because x and z are coupled by the symmetric term x^2z^2 .

After the presentation of the 3D test PES (23) by sections and equipotential surfaces, we now analyse the full 3D problem by following different curves which may be used for models of the MEP. The aim is to characterize their BPs and show their relation to VRI points of the surface.

6.2 3D minimum energy path

Taking the 2D sections for planes $z = \text{constant}$, an intuitive minimum energy path can be derived by following the 2D minima of those sections. These minima are the crossings of the corresponding RGF curves. In Fig. 5, we show a condensed picture of a relief path over this MEP (black bullets) above an (x, z) plane. We projected out the y degree of freedom by choosing at every x value the corresponding y value from the same RGF curve $E_y = 0$. Thus, we take $y = -1 - 0.5x^2$. The edge of the PES in front of the picture shows the energy profile over the RGF curve, $E_y = 0$ for $z = 0$, from SP to MIN. The BP $(0, -1, 1)$ is also the VRI point. With decreasing z we have a flat ground. A MEP goes down to the global MIN of the PES for $z = 0$. This pathway is a 3D RGF curve (2) for $k = 3$, fulfilling $E_x = E_y = 0$. However, other MEP definitions like GE or steepest descent curves result in other pathways; see below for a deeper explanation. The projected curve at the lower (x, z) coordinate plane of Fig. 5 shows the steepest descent path which starts near the BP; cf. [11, 12]. It is evident that this pathway is different to the intuitive MEP. It rather follows a GE path which also does not resemble this intuitive MEP; cf. the Sect. 6.5 below, and an analogous example in [14].

Fig. 5. 3D curvilinear surface section of $E(x, y(x), z)$ over (x, z) with $y = -1 - 0.5x^2$. The profile over the “minimum energy path” connecting the stationary-like points of a set of 2D sections at $z = \text{constant}$ (cf. Fig. 3) is shown by *black bullets*. The SP $(0, -1, 0)$, as well as the BP $(0, -1, 1)$ of that path are indicated. The BP is higher in energy by only 0.01 units. A steepest descent path is shown in the (x, z) plane. This path starts at $x_0 = 0.01$ near but outside the BP and goes to the global minimum MIN



In Fig. 6 we show the RGF solution curves of Eq. (2) in the whole 3D coordinate space. These curves are solutions omitting either the gradient part $k = 1$ to fulfill $E_y = E_z = 0$, or $k = 2$ for $E_x = E_z = 0$, or $k = 3$ for $E_x = E_y = 0$, correspondingly. For the first two cases, in the plane $z = 0$, the curves are those given in Sect. 2 and in Fig. 1B. [This is caused by the particular simplicity of the choice of surface (23) as a function in z .] In the third case the curve is $y(x) = -1 - 0.5x^2, z(x) = \pm\sqrt{1 - 0.3x^2}$. It is exactly the MEP of Fig. 5. Note: each of the curves (b) and (c) are composed of two branches. One of these branches connects the two global minima MIN without crossing the 3D SP. This means that they have to cross their BP where they cross the other branch of the same RGF curve. The corresponding BP is a VRI point of the surface.

6.3 Branin solutions

Numerical Branin solutions of the global Newton method (7) can be used for calculation of pathways between extrema, but in special cases also for the calculation of VRI points. In Fig. 2 we have shown a pattern of four numerical Branin solutions in the plane $z = 0$. The starting points are chosen near the y axis with $x_0 = \pm 0.001$ and $y_0 = -0.92$ or $= 0.492$, correspondingly. The four curves demonstrate the avoided crossing of the VRI point, which is the extraneous singularity at $(0, 0)$. The character of this avoidance is called saddle-point type [30] because of the analogy to steepest descent curves passing the neighbourhood of a SP. Taking a point on the symmetry axis as the starting point, i.e. the singular direction $x_0 = 0$ itself, we reach the VRI point as the limit. On the other hand, starting near the

minimum, we may follow a Newton flow uphill, by changing the sign in the Branin Eq. (7) from “-” to “+”. Then we search for stationary points with odd index. The VRI point divides the regions of attraction, or of repulsion, of the stationary points of the two different \pm Branin searches.

We now look for the full 3D surface (23). The gradient vector of the surface is

$$\mathbf{g}(x, y, z) = 2 \begin{pmatrix} x(0.8x^2 + y + z^2) \\ 1 + 0.5x^2 + y \\ z(0.01 + x^2) \end{pmatrix} \quad (24)$$

and the Hessian is

$$\mathbf{H}(x, y, z) = 2 \begin{pmatrix} 2.4x^2 + y + z^2 & x & 2xz \\ x & 1 & 0 \\ 2xz & 0 & 0.01 + x^2 \end{pmatrix} \quad (25)$$

The Branin formula (7) also fully works in the three dimensions of (x, y, z) . We cannot expect generally to find planar solutions like that for $z = \text{constant} = 0$. However, two further exceptional planes exist: the second symmetry plane $x = 0$ and, up to a certain degree, also the plane $y = -1$. In the latter plane, a quasi-planar behaviour of Branin solutions occur near the z axis. In Fig. 7A we show the Newton flow at $x = 0$, thus working in the symmetric (y, z) plane. This choice is due to the fact that the manifold of VRI points is the parabola $y = -z^2$ in that plane within \mathbf{R}^3 . The VRI parabola is easy to understand, if we look at the Hessian of the surface for the $x = 0$ plane:

$$\mathbf{H}(0, y, z) = 2 \begin{pmatrix} y + z^2 & 0 & 0 \\ 0 & 1 & 0 \\ 0 & 0 & 0.01 \end{pmatrix} \quad (26)$$

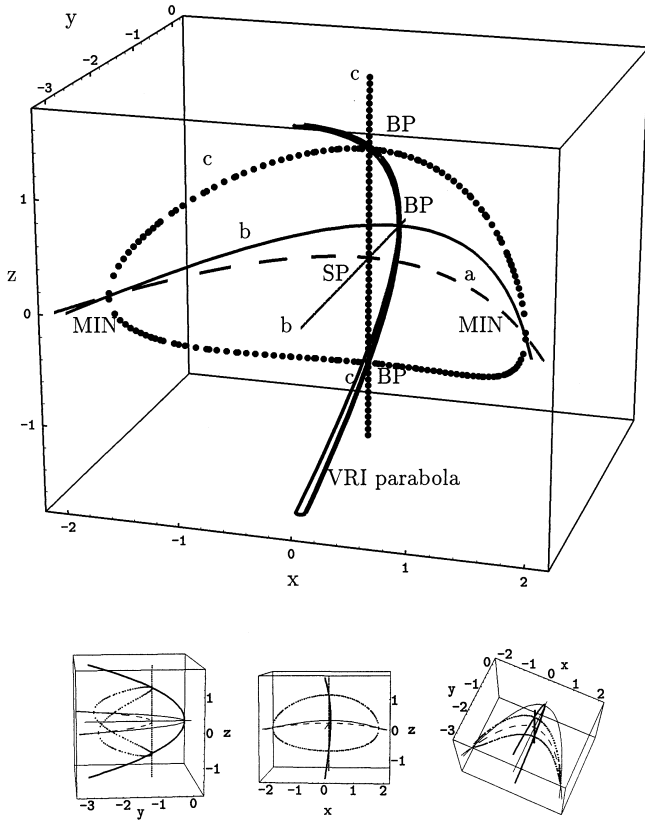


Fig. 6. Reduced gradient curves in the 3D coordinate space: They connect the global minima, MIN, the SP, and the global VRI points depicted by BP. The different RGF curves are: *a*, $E_y = E_z = 0$ (dashed); *b*, $E_x = E_z = 0$ (simple line); and *c*, $E_x = E_y = 0$ (bullets). The curves *a* and *b* are in the plane $z = 0$. The parabola of VRI points (bold) is orthogonal to that plane. The intersections of the parabola with the given special RGF curves are global points of special interest; see text. Below, three different projections of the box are shown

Taking a point on the parabola $y = -z^2$, the Hessian becomes singular, and the eigenvalue of the eigenvector $\mathbf{e}_0 (= \mathbf{e}_{\text{zero}})$ in the x direction becomes zero. The eigenvector \mathbf{e}_0 is orthogonal to the plane of interest with the gradient

$$\mathbf{g}(0, y, z) = 2 \begin{pmatrix} 0 \\ 1 + y \\ 0.01z \end{pmatrix} \quad (27)$$

This is the necessary condition for the occurrence of VRI point by the orthogonality, Eq. (6). With the initial values $(-2, 1)$, $(-1.5, 1.5)$, $(-0.5, 1)$, $(-0.2, 0.9)$, $(-0.9, 0.5)$, $(-0.9, 0.25)$, $(-0.9, 0.05)$, $(-0.9, 0)$ and $(-0.9, -0.1)$ in Fig. 7A, we always obtain sets of iteration points along straight lines. The arrows show the direction of the calculated Newton flow, which, in every case, terminate at the parabola. The rays forming the Newton flow all focus in the point $(0, -1, 0)$, the SP of the full 3D surface (23). The parabola is the one-dimensional manifold of VRI points of the surface (23).

General 3D Branin solutions of (23) close by the symmetry plane $x = 0$ are displayed in Fig. 7B. We show 4×4 Branin curves with small initial $\pm x_0$ values. The

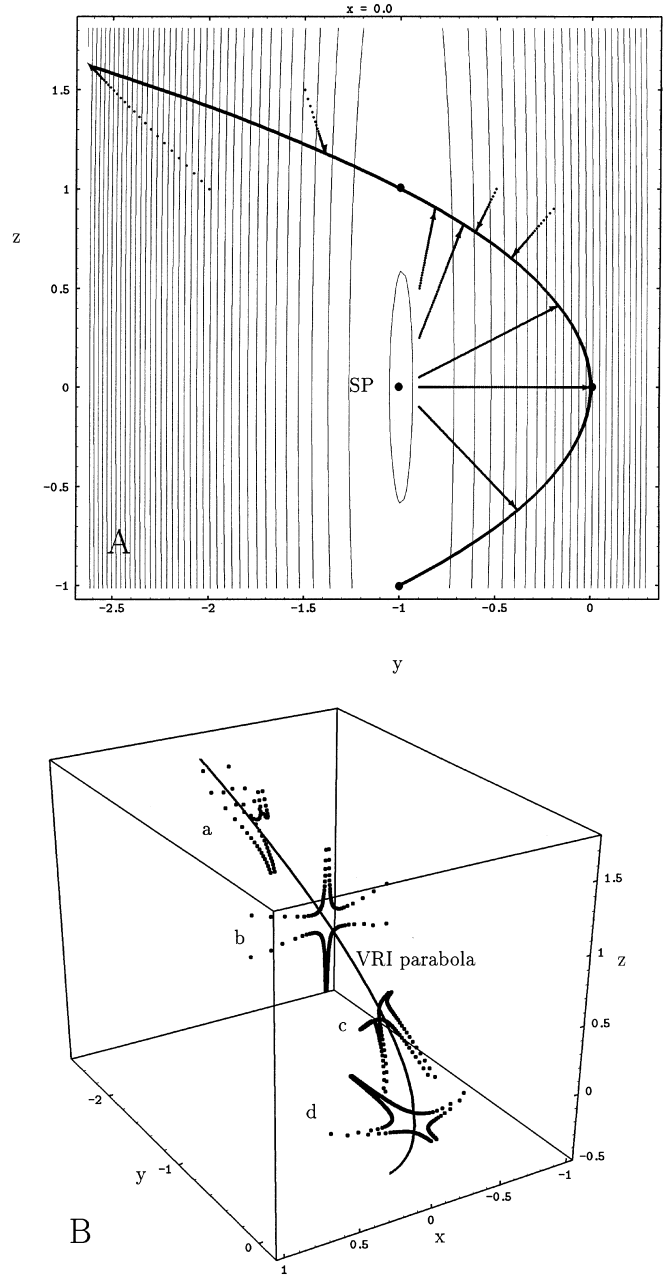


Fig. 7. A 2D section of the (y, z) plane at $x = 0$ with equipotential lines (thin), and the parabola of the VRI points of the surface. The arrows show Branin solutions converging to the extraneous singularity, the parabola of the VRI points. The SP is the “carrier” of these Branin rays. **B** 3D picture of Branin solutions in the coordinate space starting near the symmetric $x = 0$ plane of part A, now with $x_0 = \pm 0.005$ up to $x_0 = \pm 0.015$. For further explanation, see text

(y, z) pairs are a: $(-0.7, 0)$ and $(0.5, 0)$; b: $(-0.6, 0.4)$ and $(-0.3, 0.8)$; c: $(-1, 0.5)$ and $(1.2, 1.5)$; and d: $(-0.65, 1.1)$ and $(-1.8, 1.63)$. The Branin solutions (d) starting in the symmetric (x, y) plane for $z = 0$ are analogous to those in Fig. 2. These curves run in the plane, and also those in the (x, z) plane for $y = -1$ up to $|x| < 0.5$. However, the other Branin curves quickly turn off. The (x, z) plane at $y = -1$ has a dividing character for Branin solutions: it is a repellent plane. For $y > -1$, Branin curves turn off

the lime point on the parabola to run to the symmetry (x, y) plane at $z = 0$, leading finally to the global MIN. However, for $y < -1$, Branin solutions are repelled to follow the ridge of the surface uphill (in searching a stationary point of index two). In contrast, the (x, y) plane at $z = 0$ has the attractive characteristic. It is the plane where the global MIN is located and, finally, all curves starting at $y > -1$ and $x \neq 0$ are going to that MIN.

6.4 Other 2D sections

In Fig. 8, we change the point of view and consider 2D sections of (x, z) planes, where y is constant. Previously, in the case $y > 0$, the sections in (x, z) are combined by positive quadratic and quartic terms. At $y = 0$, and $z = 0$, the potential for x is pure quartic, and, therefore, it becomes very flat. For $y < 0$, the situation changes. This is shown in Fig. 8. At the x axis, two minima emerge connected by the bifurcating RGF curve $E_x = 0$. The crossing of the two different RGF curves, $E_x = 0$ and $E_y = 0$, is always at $(x, z) = (0, 0)$. This crossing point moves, for different y with $y < 0$, to a point on the ridge in Fig. 1. It does not move in x and z . However, the branching points of parts A, B and C of Fig. 8 move from $(x, z) = (0, 0)$ in the upper panel A of Fig. 8 along the positive z axis if y decreases from zero. The minima in Fig. 8A–C, on the RGF curve $E_z = 0$, are those points which would be found by the minimization in the x direction of Fig. 1 at a given value of y . The loci of these minima in the (x, z) sections also form an intuitive MEP.

A further possibility of 2D sections are (y, z) planes for $x = \text{constant}$. At first sight they seem trivial, because y and z are not coupled. The equipotential lines are pure ellipses centered at $z = 0$, and y follows the parabola $y = -1 - 0.5x^2$, being the RGF curve $E_y = 0$ of the 2D PES (4). Nevertheless, there is a peculiar situation at $x = 0.995$, or $0.01 + x^2 = 1$: the two curvatures become equal, and in 2D the whole plane would be composed by GE points [9]! However, in the full 3D coordinate space, this centre point gives a nondegenerate Hessian of the surface:

$$\mathbf{H}(0.995, -1.495, 0) = 2 \begin{pmatrix} 0.881 & 0.995 & 0 \\ 0.995 & 1 & 0 \\ 0 & 0 & 1 \end{pmatrix} \quad (28)$$

with eigenvalues 0.056, 1.937 and 1 due to the x, y coupling. Thus, we should not forget that 2D sections may give misleading illustrations for higher dimensional curvilinear surfaces.

6.5 Analysis by GEs

In order to better understand the properties of the VRI parabola, we additionally follow some gradient extremals adjacent to the VRI parabola, to the global minima and the SP. The GEs are defined without use of an arbitrary direction, in contrast to the RGF curves which are defined by a constraint. GEs satisfy the

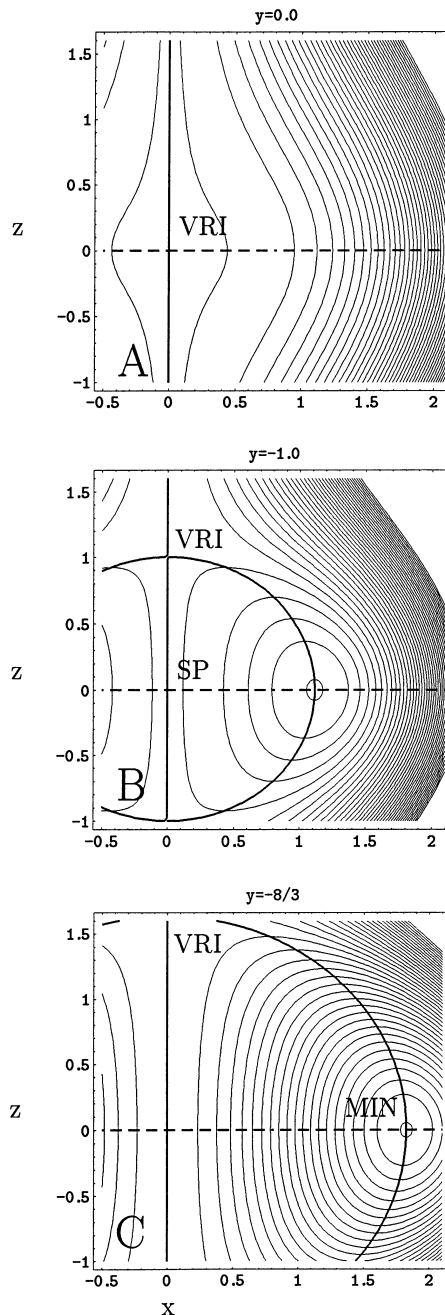


Fig. 8. 2D sections of (x, z) planes of the 3D model potential surface (23) at A: $y = 0$; B: $y = -1.0$ (SP); and C: $y = -2.67$ (MIN). 2D RGF curves are $E_x = 0$ (bold faced) and $E_z = 0$ (dashed)

condition that the value of the gradient vector along an equipotential hypersurface has an extremal point [23, 39]. This leads to the GE Eq. (20) which is simple to formulate, but the realization of a path-following procedure requires some third derivatives of the surface; cf. [13, 23, 26].

The test surface (23) is symmetric in z ; thus the $z = 0$ plane will contain some GE curves. They are shown in Fig. 9A [14]. One GE connects the two MIN $(\pm\sqrt{10/3}, -8/3)$ with the SP $(0, -1)$. Note: the GE approach to the RP between MIN and SP is different from

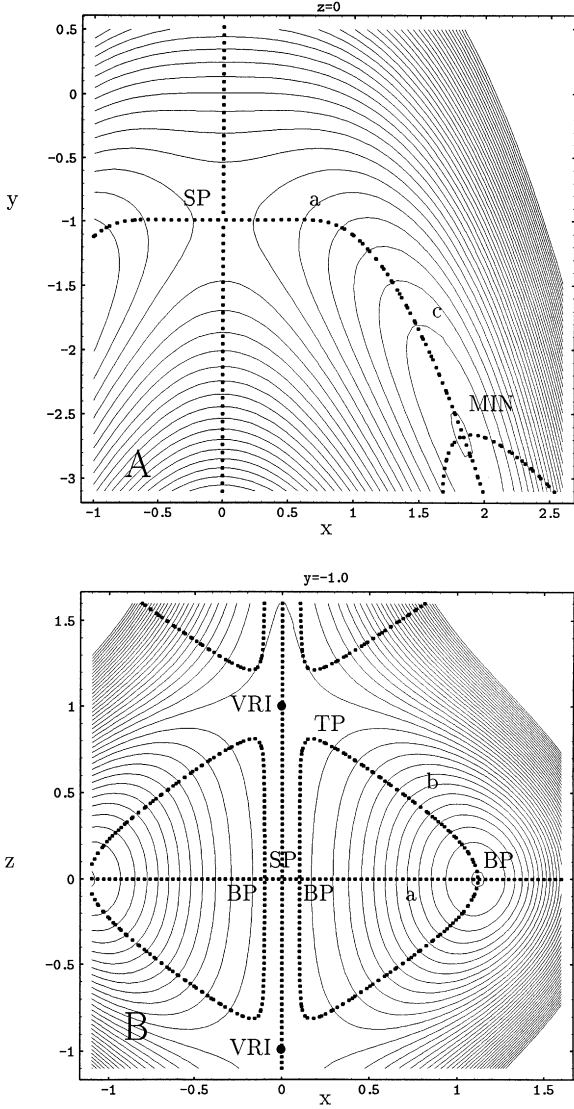


Fig. 9. **A** The 2D planar (x, y) section $z = 0$ of the surface (23) containing the 3D gradient extremals of the full 3D problem lying in that plane. **B** 2D planar (x, z) section for $y = -1$ with the local 2D GE of the surface section, which is a good approximation of the projection of the existing full 3D GE into this plane, at least for $|x| < 1$ and $|z| < 1$. The upper GEs go along a ridge, also in 3D, where they break out off this plane

the RGF curve $E_y = 0$ in Fig. 1. Orthogonal to that GE a second GE curve occurs starting in the minimum along the cirque going up the steeper slope of the bowl. The third GE runs along the y axis, which is a cirque for $y > 0$ and a cliff for $y < 0$. The calculation of these GEs can be done by using the 2D formula [9, 23]

$$E_{xy}(E_x^2 - E_y^2) + (E_{yy} - E_{xx})E_x E_y = 0 \quad (29)$$

The GE character of the y axis may be directly proved: the gradient direction is $(0, 1, 0)^T$. This is an eigenvector of the matrix \mathbf{H} at $x = 0, z = 0$.

In the full 3D case, we also find the linear GE in the z direction crossing the point $(x, y) = (0, -1)$. The gradient vector $(0, 0, 0.02z)^T$ is an eigenvector of \mathbf{H} at a pathway in the z direction. This z -axis-GE, and the y -

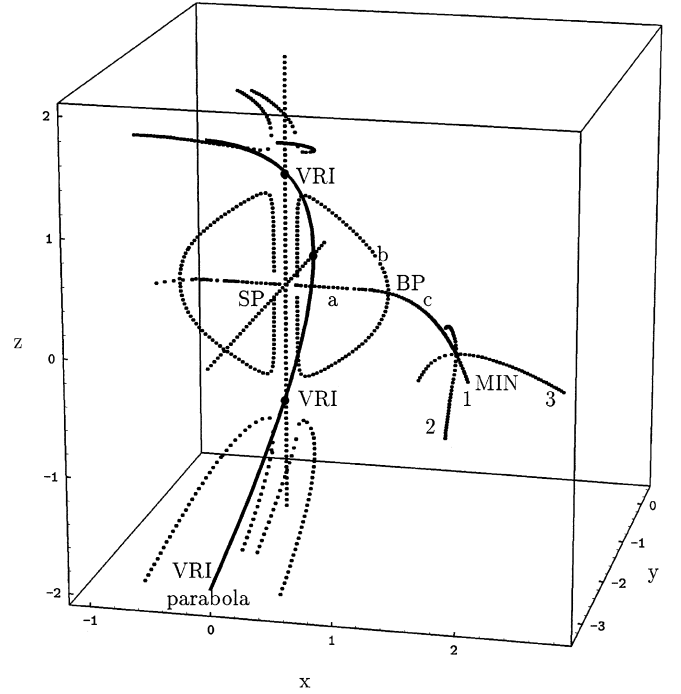


Fig. 10. Gradient extremals (dots) of the 3D polynomial surface $E(x, y, z) = 2y + y^2 + (y + 0.4x^2 + z^2)x^2 + 0.01z^2$ in 3D coordinate space, and the parabola (bold) of the VRI points of the surface. Three global VRI points are depicted by big black bullets. Two of them at $|z| = \pm 1$ are lying in the centre of turning point regions of GEs. The “true” GE-MEP from MIN to SP is not the pathway $c + a$, but the roundabout way $c + b$. The piece a of the GE is a cirque GE in an (x, z) plane; cf. Fig. 9B. Numbers at MIN depict the order of the eigenvalues of the corresponding GE curves

axis-GE given above, are the only GE curves in the (y, z) plane of $x = 0$. In Fig. 9B we show a 2D planar section of the (x, z) plane at $y = -1$. The 2D GE of that section are calculated by Eq. (29) with coordinates x, z . However, in the 3D coordinate space these curves do not represent the 3D GEs if $|x| > 0.8$ or $|z| > 1$. The GE’s “a” and “b” around zero of panel B in Fig. 9 are good projections of 3D GE curves. Note that the curve “a” is the same in A and B. The 3D BP $(0.83, -1.03, 0)$ can be observed by its 2D “projection” in Fig. 9B. It is lying on the uphill GE from the global MIN to the SP of panel A, being also a 3D saddle (see also Fig. 10). The valley GE “c” in the (x, y) plane of Fig. 9A bifurcates at the BP into the z direction. In the 3D space, the BP of the GEs is the point where the three curves “a”, “b” and “c” meet. The GE “b” of panel B then leads uphill into the direction of the global VRI $(0, -1, 1)$ explained in Fig. 5, but does not arrive at this VRI point owing to the turning point $(0.11, -1, 0.7)$. This illustrates a well-known drawback of GE curves. The VRI point region of the MEP of Fig. 5 is not well described by the crossing of GE curves; it is only crossed by the one straight line GE in the z direction but the other GEs in the (x, z) plane fail to cross the VRI region. That the other GEs come near to the VRI point may be due to the near-harmonic surface used. The upper GEs at $|z| > 1$ in B exist also in 3D, but their 2D form in Fig. 9B is not a true projection of the 3D

behaviour (compare again with Fig. 10, where the 3D GEs are illustrated in the configuration space, \mathbf{R}^3). Three GEs cross the SP. This corresponds to the picture that GEs lead along the eigenvectors at stationary points. The valley ground GE “1” passes the minimum. The GE “2” follows a way out of the $z = 0$ plane. This GE is a cirque line along the second eigenvector. GE “3” lies in an (x, y) plane, as already shown in Fig. 9A.

The GEs “c” and “a” in Fig. 10, leading from MIN to SP in the (x, y) plane for $z = 0$ (see also Fig. 9A), now obtain a new characterization due to the 3D pitchfork bifurcation at $(\pm 0.835, -1.03, 0)$ of that pathway into the (x, z) plane for $y = -1$ along GE “b”. The reason for the BP is a branching of the valley ground line which turns from the (x, y) plane into the (x, z) plane. The remaining part of the pathway, the central prong of the pitchfork, piece “a” in Fig. 10, develops as a cirque GE in 3D, leading to the SP. This GE is changed in 3D to the cirque GE along a slightly steeper ascent than the other two continuations which are valley GEs, the symmetric curve pieces “b” in Fig. 10. So, the valley path “c” bifurcates into the “a” and two symmetric “b” paths at the BP, but this BP of a GE indicates only a change of the valley: “c” is changed to “a” and changes somewhere on the path from the valley to the cirque character, but not to a ridge. Hence, this BP of GEs is not a VRI point of the surface! Note: the thick line RGF curve in Fig. 8B passes near the GE “b” of Fig. 10, but the RGF curve does not show a bifurcation in the x -axis region at the BP of the GEs.

The two symmetric 3D BPs of RGF curves, $(0, -1, \pm 1)$, are the points where the two minima of the panel A of Fig. 3 flow together to one in the middle. We call them global VRI points. Additionally, they are the points of lowest energy of the VRI parabola. They are located along the direction of the lowest positive normal mode of the SP (see Fig. 7A). These points may be identified with the term branching points of the surface. Such a global VRI point is also found at $(0, 0, 0)$. It also stands alone at the parabola by the crossing of the parabola with the y -axis GE. It is additionally the point of the parabola with the local maximum of the energy (see Fig. 7A). Other points than these three global VRI points of the parabola are not the location of GE points. The gradient vector of the surface at points of the parabola $y = -z^2, x = 0$, is the vector $2(0, 1 - z^2, 0.01z)^T$. It is generally not an eigenvector of the (constant) Hessian

$$\mathbf{H}(0, -z^2, z) = 2 \begin{pmatrix} 0 & 0 & 0 \\ 0 & 1 & 0 \\ 0 & 0 & 0.01 \end{pmatrix} \quad (30)$$

which is only the case at the three special points $(0, -1, \pm 1)$ and $(0, 0, 0)$. Although the gradient always is orthogonal to the zero eigenvector of this Hessian, namely the $(1, 0, 0)^T$ direction orthogonal to the VRI parabola in \mathbf{R}^3 , it generally is not an eigenvector itself. This becomes true in the case of simple 2D treatments: there is only one direction orthogonal to a given zero eigenvector. In a higher dimensional case, the gradient may rotate orthogonal to the zero eigenvector between the other eigenvectors of the Hessian. Thus, the gradient

exists in a subspace orthogonal to the zero eigenvector. Collins [40] says: “...GE paths do have the interesting feature that they pass through VRI points”. The 3D example shows that this is only true sometimes, namely for the above so-called global VRI points.

7 Discussion

A number of special points of the surface (23) are defined by crossing of the curves calculated. These may be the points of chemical or spectroscopic interest:

1. Global minima are the points $(\pm\sqrt{10/3}, -8/3, 0)$, which correspond to stable molecular geometries. The eigenvalues of the Hessian are all positive: 10.9996, 3.3432 and 0.6. Three GEs cross these minima, leaving them along the directions given by the three eigenvectors.
2. The saddle point of index one is at $(0, -1, 0)$. It is the pass along the valley GE between the two minima in the symmetry plane $z = 0$ (see Fig. 9A). It is also the energy maximum along the valley GE between the two BPs in the plane $y = -1$ in Fig. 9B, because the cirque GE “a” changes near the SP again into the valley GE. The eigenvalues of the surface Hessian at the SP are $-1, 1$, and 0.01 , where the negative eigenvalue describes the transition vector (x direction). Three GEs are crossing each other. A RGF curve in the full 3D, $E_y = E_z = 0$ (the dashed curve in Fig. 6), connects the global MIN with the SP.
3. The point $(0, 0, 0)$: one eigenvalue is zero, the other two are positive, and the orthogonality condition of Eq. (6) is fulfilled. Thus, it lies on the 1D VRI manifold and on the horizontal straight line GE through $x = 0, z = 0$ (y axis). The point is the vertex of the parabola of VRI points. It is not a stationary point, but it is a BP of the 3D RGF curve $E_x = E_z = 0$ (of the branches “b” in Fig. 6).
4. The points $(0, -1, \pm 1)$: as in 3, one eigenvalue is zero, the other two are positive, and the orthogonality condition of Eq. (6) is fulfilled. Thus, they are again VRI points. They are crossing points with the straight line GE through $x = 0, y = -1$ along the z direction. Because for $z \neq 0$ the gradient does not vanish, the two points do not form stationary points. They are the BPs of the branches of the 3D RGF curve with $E_x = E_y = 0$ (the bullet curve in Fig. 6).

What meaning do these global VRI points have? In point $(0, 0, 0)$ a change of the character of the surface begins (in the $z = 0$ plane) if one looks at the other two degrees of freedom, (x, y) : a downward cirque coming from positive y changes into a cliff along its pathway to the SP. The branches of the RGF curve “simulate” two valleys, cf. Figs. 1B and 3A, bypassing the SP. For $z \neq 0$ the BP of the RGF occurs at lower values of y . The VRI point in Fig. 1A is the limiting VRI point in the y direction seen over all z values. Figure 4 shows that the surface in the neighbourhood of the point $(0, 0, 0)$ in panel C is the last convex equipotential surface. Before this BP $(0, 0, 0)$, thus for $y > 0$, the corresponding equipotential surfaces are convex, but after the BP two

small swellings emerge in front of the panels A or B. They cause a concavity behaviour of the equipotential surface in the x direction. The BP $(0, 0, 0)$ is that point where the concavity begins.

On the other hand, at the BPs $(0, -1, \pm 1)$, the two minima in the corresponding (x, y) plane, see Fig. 3, disappear and flow together to one single minimum. The planes $z = \pm 1$ are the limits of the existence of the two “isomers”. In Fig. 4A and B, we observe a sudden change of the equipotential surface taken at the SP level in A, to the BP $(0, -1, \pm 1)$ level in B by closing the canyon between the two lobes still visible in panel A. For increasing $|z| > 1$ a summit in the z direction of panel C emerges. Thus, the BP region is again the region where local concavity changes into convexity, along the z direction.

The character of the VRI manifold is well understood by RGF curves, but only three points of that manifold, $(0, -1, \pm 1)$ and $(0, 0, 0)$ are characterized by a crossing of the manifold of VRI points with a GE curve. These points on the GE-MEPs form the BPs of “chemical or “spectroscopic” interest. Note that every point of the VRI parabola is a BP of a corresponding RGF search direction \mathbf{r} in Eq. (16); compare Fig. 7B. This leads to the conception of a manifold of VRI points – in this case of a one-dimensional curve.

Intuitive thinking would prefer the MEP of Fig. 5 to be the static path connecting the global VRI points, $(0, -1, \pm 1)$, and the global minima, MIN, of the surface. It is constructed by connecting the locus of crossing RGF curves in $z = \text{constant}$ planes. The GE procedure does not accommodate this intuition. The valley GE “b” of Fig. 9B does not cross the global VRI point owing to its turning point. However, the turning point region of this GE also characterizes the VRI region. The downward pathway “b” of the GE from TP to the right BP of the panel B goes roughly parallel to the intuitive MEP. A steepest descent path also goes along this course. However, the BP behaviour of the GE curves between the planes (x, z) and (x, y) is not mirrored by the intuitive MEP. So, at a deeper view, the GEs give a better insight into the finer structure of the surface valleys and cirques, or ridges and cliffs. Bifurcation points of RGF curves represent VRI points. Thus, if RGF fortunately follows the MEP, as along the positive y axis in Fig. 1, then VRI forms also the MEP branching point. The combination of symmetry adapted RGF curves and of GE curves allows us to localize the global structure of the surface as well as the exact pathways and bifurcations of possible reaction valleys.

A 1D manifold of VRI points, i.e. a curve, is obtained in \mathbf{R}^3 coordinates. This makes it evident that in higher dimensional PES applications, as is the usual case in theoretical chemistry, a whole manifold of VRI points does exist. It maximally reaches the dimension $n - 2$, where n is the dimension of the surface [30]. This “manifold character” may be compared with the MEP always understood as a curve.

Appendix A: proof of the VRI character of a zero product of adjoint and gradient

We assume $\mathbf{g} \neq 0$. The statement is: if Eq. (6) is fulfilled then the gradient \mathbf{g} is orthogonal to a zero eigenvector \mathbf{e}_0

of the Hessian, \mathbf{H} . If $\mathbf{e}_1, \mathbf{e}_2$ and $\mathbf{e}_3 (= \mathbf{e}_0)$ are the eigenvectors of \mathbf{H} with eigenvalues λ_1, λ_2 and $\lambda_3 (= 0)$, then they are also the eigenvectors of \mathbf{A} but with the eigenvalues $\mu_1 = \lambda_2 \lambda_3$, $\mu_2 = \lambda_1 \lambda_3$ and $\mu_3 = \lambda_1 \lambda_2$. This is due to the equation

$$\mathbf{H} \mathbf{e}_i = \lambda_i \mathbf{e}_i, \quad (31)$$

Thus, by multiplication with the adjoint matrix we get

$$\mathbf{A} \mathbf{H} \mathbf{e}_i = \text{Det}(\mathbf{H}) \mathbf{e}_i = \lambda_i \mathbf{A} \mathbf{e}_i \quad (32)$$

with

$$\text{Det}(\mathbf{H}) = \lambda_1 \lambda_2 \lambda_3 \quad (33)$$

If \mathbf{H} has the zero eigenvalues $\lambda_3 = 0$ then \mathbf{A} has two zero eigenvalues, $\mu_1 = 0$ and $\mu_2 = 0$. Expressing \mathbf{g} by the three eigenvectors

$$\mathbf{g} = a_1 \mathbf{e}_1 + a_2 \mathbf{e}_2 + a_3 \mathbf{e}_3 \quad (34)$$

gives the relation

$$\mathbf{A} \mathbf{g} = a_3 \lambda_1 \lambda_2 \mathbf{e}_3 \quad (35)$$

if $\lambda_3 = 0$. If now \mathbf{g} is orthogonal to \mathbf{e}_3 then a_3 has to be zero, and if a_3 is zero then Eq. (6) is satisfied.

Note that the proof also shows that an inflection point of an energy profile along a valley ground generally is not an extraneous singularity, in the sense of VRI, because \mathbf{g} is not orthogonal to \mathbf{e}_3 , and so $a_3 \neq 0$. The curvature of the energy profile along the MEP is not relevant for the VRI problem!

Appendix B: a series of cusps

The orthogonality condition of Eq. (6) for an eigenvector \mathbf{e}_0 of \mathbf{H} to the zero eigenvalue is satisfied by points of the VRI parabola $y = -z^2$ at $x = 0$. However, Eq. (6) has still a second solution. It is also fulfilled by the points of the curve

$$(x(t), y(t), z(t)) = (t, (0.01 - 3.017t^2 - 0.5t^4)/(0.01 + t^2), \sqrt{-1 + 0.3t^2}) \quad (36)$$

where $x = t$ is used as the curve parameter. At any point of that curve there is one eigenvalue of \mathbf{H} equal to zero, and the gradient of the surface is orthogonal to the zero eigenvector. However, it is not the region where the crest of the ridge changes into the valley ground, but it is a special sort of flank line: it is part of the border between the regions of ridge and valley. Of course, in 3D, this border is a 2D surface. Curve (36) picks out special points of this surface where Eq. (6) is also fulfilled. Curve (36) is shown in Fig. 11 in the quadrant of positive (x, z) of the configuration space \mathbf{R}^3 . At the four points $\mathbf{a} = (\sqrt{10}/3, -14/3, 0)$, $\mathbf{b} = (2.2, -5.42, 0.67)$, $\mathbf{c} = (2.5, -6.13, 0.94)$ and $\mathbf{d} = (2.8, -6.93, 1.16)$, a frame of three vectors is fixed. The large one is the scaled gradient of the surface at the corresponding point. The small vector with a vector head is the normalized zero eigenvector of that point, and the stick without a vector head is the normalized cross product of the two former directions called below “vector **cross**”. The region of that curve is outside of the region of the stationary points as well as

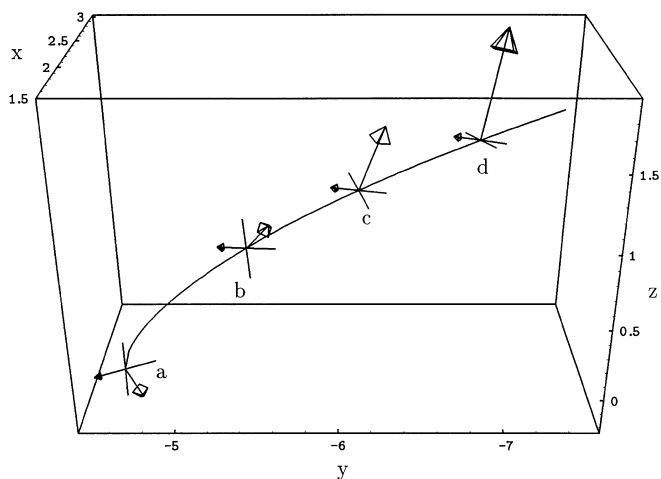


Fig. 11. 3D curve of cusps also fulfilling the VRI equation. The vectors fixed at four points are gradients of the full surface and zero eigenvectors of the Hessian, and also the cross products of the two vectors of the corresponding curve point

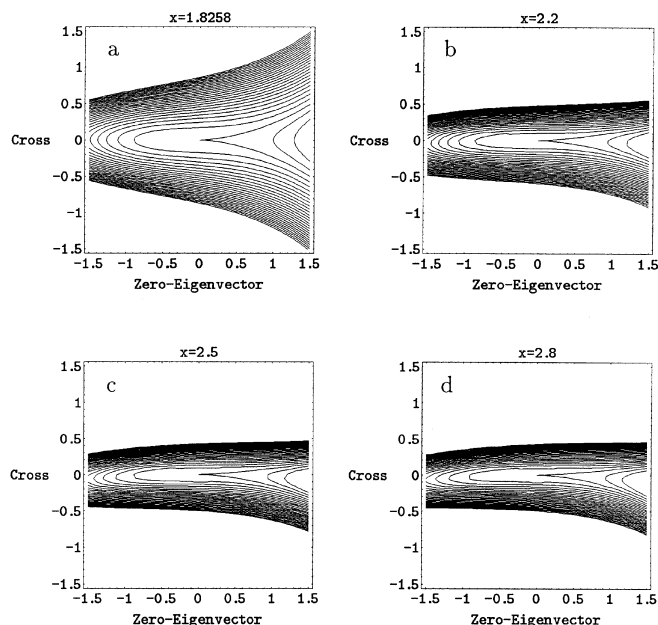


Fig. 13. The 2D planes $(\mathbf{e}_0, \mathbf{cross})$ of the surface (23) with equipotential lines. The panels correspond to the cases a to d of Fig. 11 where the point $(0, 0)$ is the corresponding curve point. The level line through this point is a cusp. The distance between two lines is 0.1 units

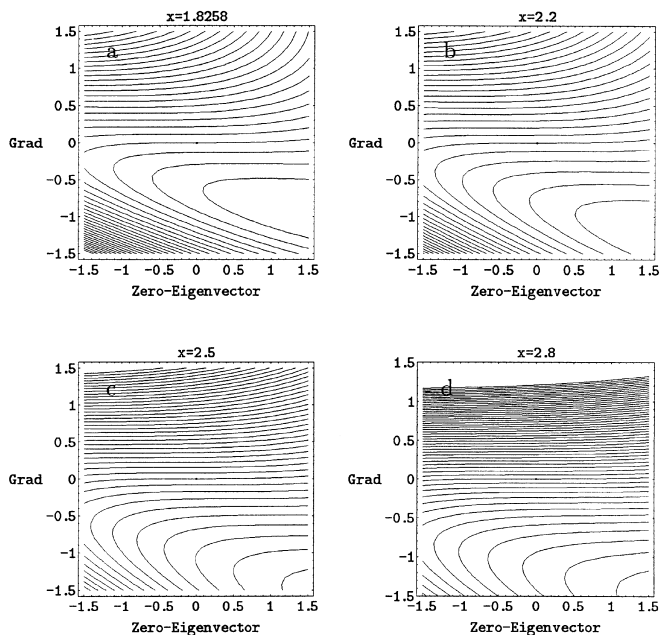


Fig. 12. The 2D planes $(\mathbf{e}_0, \mathbf{g})$ with equipotential lines of the surface (23). The panels correspond to the cases a to d of Fig. 11 where the flat $(0,0)$ is the corresponding curve point. The distance between two lines is one unit

the global VRI points, which are treated in the Figs. 1–10. At point a, the curve (36) begins as its vertex. The gradient vector as well as the zero eigenvector lie in the (x, y) plane, and the “vector cross” points into the pure z direction. In all other cases, the frame is rotated. We treat the test surface by using 2D sections to understand the curve (36) in Figs. 12 and 13. The 2D surface shows a normal pattern of level lines in the plane $(\mathbf{e}_0, \mathbf{g})$ shown in Fig. 12, and also in the plane $(\mathbf{cross}, \mathbf{g})$ where the level lines are simple convex curves. The special property of the level lines at point $(0,0)$ in Fig. 12, within the point of

the curve (36), is the zero curvature by calculation corresponding to Eq. (6), but the zero eigenvalue is due to a cubic inflection point. $(0,0)$ is that point where the ridge of the upper right-hand side of the panels ends and the valley of the lower left-hand side begins.

Some levels show a quite strange shape shown at the point $(0,0)$ in Fig. 13. The corresponding panels are planes $(\mathbf{e}_0, \mathbf{cross})$ at the points a–d of Fig. 11. The 2D surface is a valley ascending from the right- to the left-hand side with decreasing value of the coordinate ξ along the zero eigenvector. The level line through the point $(0,0)$ is a cusp. The shape of this curve is a subject of catastrophe theory; cf. also [9]. Its germ is the function $\xi^3 = a\eta^2$ for $\xi > 0$ along \mathbf{e}_0 , η along \mathbf{cross} , and a is a constant. The cusps of Fig. 13 are more complicated functions. The surface over the given planes has the form of a chair. At one sitting, exactly one level line shows the grotesque cusp shape. All other levels before and after the cusp are usually curvilinear level lines.

Acknowledgements. Our work was made possible through the financial support of the Deutsche Forschungsgemeinschaft. We are grateful to Chris Whitrow for critically reading the manuscript. We thank the referees for nice comments.

References

1. Laidler K (1969) Theory of reaction rates. McGraw-Hill, New York
2. Truhlar DG (1995) In Heidrich D (ed) The reaction path in chemistry: current approaches and perspectives. Kluwer, Dordrecht, p 229

3. Metiu H, Ross J, Silbey R, George TF (1974) *J Chem Phys* 61:3200
4. Valtazanos P, Ruedenberg K (1986) *Theor Chim Acta* 69:281
5. Kraus WA, De Pristo AE (1986) *Theor Chim Acta* 69:309
6. (a) Minyaev RM (1994) *Russ Chem Rev* 63:883; (b) Minyaev RM (1995) *Zh Fiz Khim* 69:408.
7. Basilevsky MV (1987) *Theor Chim Acta* 72:63
8. Quapp W (1989) *Theor Chim Acta* 75:447
9. Heidrich D, Kliesch W, Quapp W (1991) *Properties of chemically interesting potential energy surfaces*. Springer, Berlin Heidelberg New York
10. (a) Tachibana A, Okazaki I, Koizumi M, Hore K, Yamabe T (1985) *J Am Chem Soc* 107:1190; (b) Tachibana A, Fueno H, Yamabe T (1986) *J Am Chem Soc* 108:4346
11. Schlegel HB (1994) *J Chem Soc Faraday Trans* 90:1569
12. Quapp W (1994) *J Chem Soc Faraday Trans* 90:1607
13. Ruedenberg K, Sun J-Q (1994) *J Chem Phys* 100:5836
14. Quapp W, Imig O, Heidrich D (1995) In Heidrich D (ed) *The reaction path in chemistry: current approaches and perspectives*. Kluwer, Dordrecht, p 137
15. Paz JJ, Moreno M, Lluch JM (1995) *J Chem Phys* 103:353
16. (a) Taketsuga T, Hirano T (1993) *J Chem Phys* 99:9806; (b) Taketsuga T, Hirano T (1994) *J Mol Struct (Theochem)* 130:169; (c) Liao JL, Wang HL, Xin HW (1995) *Chin Sci Bull* 40:566; (d) Taketsuga T, Gordon MS (1995) *J Chem Phys* 103:10042; (e) Yanai Y, Taketsuga T, Hirano T (1997) *J Chem Phys* 107:1137
17. (a) Collard KG, Hall GG (1977) *Int J Quantum Chem* 12:623; (b) Basilevsky MV (1977) *Chem Phys* 24:81
18. Fukui K (1970) *J Phys Chem* 74:4161
19. (a) Tachibana A, Fukui K (1978) *Theor Chim Acta* 49:321; (b) Quapp W, Heidrich D (1984) *Theor Chim Acta* 66:245
20. Garrett BC, Redmon MJ, Steckler R, Truhlar DG, Baldrige KK, Bartol D, Schmidt MW, Gordon MS (1988) *J Phys Chem* 92:1476
21. (a) Baker J, Gill PMW (1988) *J Comput Chem* 9:465; (b) Marcus RA (1991) *J Phys Chem* 95:8236; (c) Minyaev RM, Wales DJ (1994) *J Chem Soc Faraday Trans* 90:1831; (d) Garavelli M, Calani P, Bernardi F, Robb MA, Olivucci M (1977) *J Am Chem Soc* 119:6891; (e) Shaik S, Danovich D, Sastry GN, Ayala PY, Schlegel HB (1977) *J Am Chem Soc* 119:9237; (f) Bosch E, Moreno M, Lluch JM (1989) *Chem Phys Lett* 160:543
22. Basilevsky MV, Shamov AG (1981) *Chem Phys* 60:337, 60:347
23. Hoffman DK, Nord RS, Ruedenberg K (1986) *Theor Chim Acta* 69:265
24. Sun J-Q, Ruedenberg K (1993) *J Chem Phys* 98:9707
25. Jørgensen P, Jensen HJA, Helgaker T (1988) *Theor Chim Acta* 73:55
26. Jensen F (1995) *J Chem Phys* 102:6706
27. Bondensgård K, Jensen F (1996) *J Chem Phys* 104:8025
28. Quapp W, Hirsch M, Imig O, Heidrich D (1998) *J Comput Chem* 19:1087
29. Guest MF, Fantucci P, Harrison RJ, Kendric J, van Lenthe JH, Schoeffel K, Sherwood P (1993) *GAMESS-UK program*. CFS, Daresbury Laboratory, UK
30. Jongen HTh, Jonker P, Twilt F (1987) In: Guddat J et al. (eds) *Parametric optimization and related topics*. Akademie Verlag, Berlin, p 209
31. (a) Rothmann MJ, Lohr LL Jr (1980) *Chem Phys Lett* 70:405; (b) Scharfenberg P (1981) *Chem Phys Lett* 79:115; (c) Scharfenberg P (1982) *J Comput Chem* 3:277
32. Williams IH, Maggiora GM (1982) *J Mol Struct (Theochem)* 89:365
33. Wolfram S (1993) *Mathematica, Version 2.2*, Wolfram Research Inc., Champaign, USA
34. Branin FH (1972) *IBM J Res Dev* 504
35. (a) Allgower EL, Georg K (1990) *Numerical continuation methods – an introduction*. Springer, Berlin Heidelberg New York; (b) Schwetlick H (1984) *Computational mathematics*. PWN, Warsaw, p 623
36. Quapp W (1995) In: Heidrich D (ed) *The reaction path in chemistry: current approaches and perspectives*. Kluwer, Dordrecht, p 95
37. (a) Makri N, Miller WH (1989) *J Chem Phys* 91:4026; (b) Shida N, Barbara PF, Almlöf JE (1989) *J Chem Phys* 91:4061; (c) Komatsuzaki T, Nagaoka M (1996) *J Chem Phys* 105:10841; (1997) *Chem Phys Lett* 265:91; (d) Došlić N, Kühn O, Manz J (1998) *Ber Bunsenges Phys Chem* 102:292
38. (a) Botschwina P, Rosmus P, Reinsch E-A (1983) *Chem Phys Lett* 102:299; (b) Botschwina P, Seeger S, Mladenovich M, Schatz B, Horn M, Schmatz S, Flügge J, Oswald R (1995) *Int Rev Phys Chem* 14:169; (c) Liedl KR, Kroener RT, Rode BM (1995) *Chem Phys Lett* 246:455; (d) Benderskii VA, Vetoshkin EV, Grebenshchikov SYu, von Laue L, Trommsdorf HP (1997) *Chem Phys* 219:119; (e) Schmidt RG, Brickmann J (1997) *Ber Bunsenges Phys Chem* 101:1816
39. (a) Panciř S (1975) *Collect Czech Chem Commun* 40:1112; (b) Rowe DJ, Ryman A (1982) *J Math Phys* 23:732; (c) Basilevsky MV (1982) *Chem Phys* 67:337
40. Collins MA (1996) In: Prigogine I, Rice SA (eds) *Advances in chemical physics*, vol 93. Wiley, New York, p 389